High Dynamic Range Image Composition Using a Linear Interpolation Approach

Yun-Te Lin
National Center for High-Performance Computing, NARLabs, Hsinchu, Taiwan
National Chung Hsing University, Taichung, Taiwan
lsi@nchc.org.tw

Ming-Long Huang
National Chung Hsing University, Taichung, Taiwan
sk8board@ms34.hinet.net

*Chung-Ming Wang**
National Chung Hsing University, Taichung, Taiwan
cmwang@cs.nchu.edu.tw

Abstract—Linear interpolation is a simple yet effective technique for image composition which works wells for low dynamic range (LDR) images with a fixed range of pixel values. However, it cannot provide good performance for high dynamic range (HDR) images because a high luminance image usually dominates the composition result. This paper proposes a novel algorithm for HDR composition using the linear interpolation. Our scheme decomposes HDR images to be composed into three layers where a linear interpolation can be applied on each layer individually that has been normalized. The algorithm contains three steps including the image decomposition, the image feature composition, and finally the HDR map estimation and image re-rendering. Experimental results show that the proposed approach can produce informative HDR composition images balancing the influence caused by the low or high luminance and preserving the contrast, colors, and salience. The comparison demonstrates that our scheme outperforms the current state-of-the-art methods.

Keywords—High dynamic range images, exposure, composition, linear interpolation, tone-mapping, decomposition.

I. INTRODUCTION

Digital image is closely related to our daily life due to the universal of digital cameras. We may compose two or more images within an image to produce a meaningful image for artistic and esthetic rendition. In general, we call such a procedure the image composition. Composing different scenes or objects within an image is fundamental in movie industry and advertisement design. Linear interpolation method is one of commonly adopted techniques [5]. This method has proven to be very effective for low dynamic range (LDR) images, such as bitmap image format for instance, where the pixel value is normally in a fixed range within [0, 1].

In recent years, interest in high dynamic range (HDR) images has increased dramatically [4] [9] [14] [18] [19]. The dynamic range of a scene is the contrast ratio between its brightest and darkest parts. An HDR image with pixels being represented by a floating point can accurately represent the wide range of intensity levels found in real scenes, ranging from direct sunlight to deepest shadows, in order to exhibit the accurate fidelity of a real scene.

Unfortunately, the linear interpolation method is not applicable for high dynamic range (HDR) image composition. This is because the features of dynamic range lead to pixel values with much variety of dynamic range scattering from 1 to as high as 20 or even higher. In general, HDR images can be categorized into three types: high, mid, and low exposure [8].The floating point value of most pixels in a low exposure image may be smaller than 0.1, while the pixel values in a high exposure one may be larger than 100. If we attempt to linearly compose two different types of HDR images, the composite result is surely dominated by the high exposure HDR images. Consequently, the resultant HDR image may contain information revealed mainly from the dominated HDR image, violating the experiences and anticipated effects of using the linear composition

In this paper, we present an effective method to solve the problem of HDR image composition. Our method involves three steps. First, in the image decomposition step, an HDR image is decomposed as three features; that is, base layer, color layer and detail layer, respectively. Next, in the mage feature composition step, a linear interpolation technique is adopted to compose HDR images in three layers, where we can flexibly adopt different weights to produce versatile composition results. Finally, in the HDR map estimation and image re-rendering, we estimate the magnitude of the exposure in the newly composited HDR image and employ a map estimation method to re-render the HDR image producing the final composition results. Experimental results show that our algorithm can produce a more informative HDR composition result outperforming other approaches.

This paper is organized as follows. We review previous approach for the LDR image composition. We then describe our proposed algorithm in Section 3. Experimental results and comparison are presented in Section 4, followed by a conclusion given in the final section.

II. RELATED WORKS

Grundland *et al*. pioneered the work for LDR image composition [6]. They observed that when a linear interpolation method is performed onto the grayscale images, the composite result is acceptable. However, if the same scheme is targeted for color images, the side effects of contrast loss and color fading occurred which reduces the visibility of image details.

978-1-5090-0806-3/16/$31.00 copyright 2016 IEEE
ICIS 2016, June 26-29, 2016, Okayama, Japan

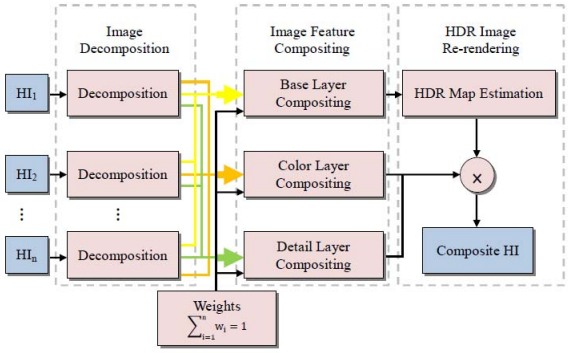

Figure 1. The flowchart of high dynamic range image composition.

To cope with the problem, they presented three solutions which were based on the statistical analysis, vector algebra, and information theory. These solutions offer benefits to preserve the image contrast, color variations, and image salience. Although the contrast preserving method preserves better contrast within the composite result, the side effect of color fading remains in the composition results.

Later, a non-linear image composite technique was proposed to improve the color fading problem [7]. In this method, they combined the Laplacian pyramid with a newly defined sign-weighted power mean function. Their method provides another advantage in image stitching [16] and image fusion [17].

We consider that even using non-linear interpolation approach for HDR images, the HDR composition results is not acceptable. This is due to the fact that since HDR images have a variety of exposures, if we compose two HDR images, the image content with a high exposure would cover over that with the low exposure. This leads to that the overall appearance in the composite image consists of saliency from a high exposure image and little information is shown for the details with low exposure. In other words, a composite HDR image is not able to exhibit the content of both low and high exposure simultaneously. Consequently, it is a challenge to design and develop an effective algorithm which can provide benefits for HDR image composition for the image community.

III. HDR Image Composition

We describe our proposed HDR image composition algorithm using a linear interpolation in this section. We consider that an HDR image (I) is composed by three layers, I = CL * BL * DL, where CL presents the color layer, BL is the base layer, and DL denotes the detail layer. Our aim is to decompose these three layers from an image and then transform layers into an applicable uniform numerical domain on which we are able to process each layer individually to accomplish the HDR image composition.

The flowchart of our scheme is illustrated in Fig. 1 which has three primary processes: image decomposition, image feature compositing, and HDR image re-rendering. First, each HDR image to be composed is decomposed into three feature layers, as shown in Fig. 1, which include the base layer, color layer, and detail layer. Next, we adopt the linear interpolation method at each layer individually and produce the composite features, as shown in Fig. 2. This produces the composite base layer BL_c, composite color layer CL_c, and composite detail layer DL_c. Finally, we estimate the reconstruction HDR map, HMap, via the composite base layer. We then combine the color and detail layers with the HMap and re-render the final composite HDR image. We detail each process in the following subsections.

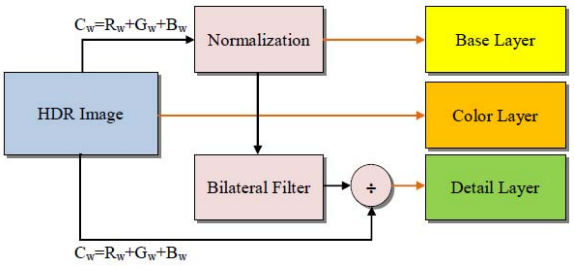

Figure 2. The flowchart of producing three composite layers.

A. Color Layer

The Human Visual System (HVS) contains light sensitive cone cells enabling us to recognize colors. These cells can be categorized into three types: red cone cells, green cone cells, and blue cone cells. These three colors are also known as the triple primary channels.

HDR images record a wide range of color information and are usually represented by floating point values so as to closely measure the chromatic variations of real world environment. Mathematically, we can employ Eq. (1) to describe the colors of an HDR image at a pixel (i, j), where the suffix w presents real world environment.

$$C_w(i, j) = R_w(i, j)+G_w(i, j) + B_w(i, j). \quad (1)$$

We remark that all color intensities of an image is considered as the color layer. Thus, we can further derive the influential ratios corresponding to the triple primary at each pixel (i, j), as shown in Eq. (2). These ratios are in the range between 0 and 1.

$$\begin{aligned} r_w(i, j) &= R_w(i, j)/C_w(i, j). \\ g_w(i, j) &= G_w(i, j)/C_w(i, j). \\ b_w(i, j) &= B_w(i, j)/C_w(i, j). \end{aligned} \quad (2)$$

The benefit of adopting these ratios for HDR composition is that we can immediately compose color intensities using linear interpolation method. We show in Fig. 3 the tone-mapped images Bush (low exposure) and Sunset (high exposure) and their color layers. We remark that the color layer indeed represents the chromatic information in the triple primary channels.

B. Base Layer

We have represented the color intensities by the sum of the triple primary. Since an HDR image has different exposure causing the difficulty for conducting the linear interpolation, we normalize the luminance of an HDR image to derive the base layer to accomplish the HDR composition.

We adopt five steps to derive the base layer. In particular, we adopt the approach suggested by Reinhard *et al*. [14] to

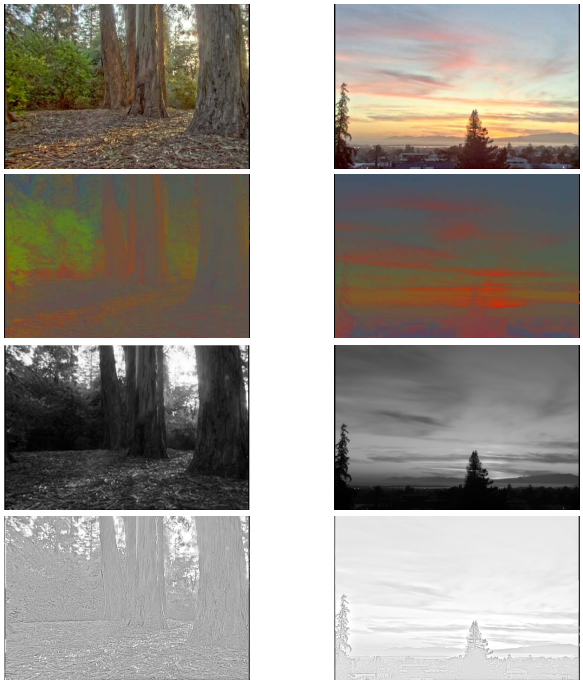

Fig. 3. An illustration of the tone-mapped Bush and Sunset images (top row), color layer (second row), base layer (third row) and detail layer (bottom row). Note that our algorithm can obtain the details in the regions with similar luminance variations.

produce the mapped value $C_m(i,j)$ using Eqs. (3), (4) and (5). We then compute the square value of the white point for the given HDR image followed by deriving the final base layer for each pixel $C_n(i,j)$. We detail five steps below.

First, we determine the luminance of the pixel (i, j), denoted by $C_w(i,j)$, using (3), where (w_r, w_g, w_b) = (0.2989, 0.5870, 0.1140). Then, we compute the average luminance C_{av} using (4), where δ is a small value (10^{-5}) to avoid the singularity of the C_w value. In the third step, we derive the mapped value C_m, where α is automatically estimated by the maximal (C_{max}) and minimal (C_{min}) luminance of the input HDR image. In the fourth step, we determine the white point of the input HDR image. We remark that a white point of using the constant 1.5 is a suitable choice [14] which produces a reasonably enhanced display image for a low dynamic range image of 5 zones. In addition, it is reasonable to adopt the constant 10 for the square value since high dynamic range images tend to consist of more than 11 zones in the Zone system [1]. Once the white point is available, we adopt Eq. (7) to derive the final base layer for each pixel (i, j) by referring to the mapped value $C_m(i,j)$ that has been derived.

$$C_w(i,j)=w_r*R(i,j)+w_g*G(i,j)+w_b*B(i,j). \quad (3)$$

$$C_{av} = e^{\{\frac{1}{n}\sum_{i,j}^{n}[\log_e(C_w(i,j)+\delta)]\}}. \quad (4)$$

$$C_m(i,j) = \alpha \times C_w(i,j)/C_{av}. \quad (5)$$

$$C_{white}^2 = (1.5)^2 \times 2^{[\log_2(C_{max}/C_{min})^2-10]}. \quad (6)$$

$$C_n(i,j) = \frac{C_m(i,j)\times[C_{white}^2+C_m(i,j)]/C_{white}^2}{C_m(i,j)+1.0}. \quad (7)$$

We show in Fig. 3 the tone-mapped Bush and Sunset images and the color and base layers. It is interesting to point out that a base layer provides an efficient mechanism because it allows us to make use of the low, middle and high exposure parts when composing the HDR images.

C. Detail Layer

An investigation targeted for low dynamic range images [6] [7] indicated that when we conduct the image composition, the visibility of image details is decreased due to the contrast loss and color fading effects. Consequently, we need to preserve as many as possible the detailed information stored in the high dynamic range images. We describe our approach of using the bilateral filter to develop the detail layer.

The bilateral filter is a fast, non-iterative technique, and has been applied to tone-mapping [3] [14]. The development of our detail layer also builds on the bilateral filter. We describe the fundamentals of the bilateral filter followed by presenting our approach to develop the detail layer.

The bilateral filter averages pixels that are spatially near one another and have similar intensity values [13] [20]. Combining a classic low-pass filter with an edge stopping function, it attenuates the filter kernel weights when there is a large intensity difference between pixels. We adopt the bilateral filter to develop the detail layer using the following two steps. First, the bilateral filter computes the value of pixel *s* denoted by $BF_s[C_n(i,j)]$ as shown in Eq. (8). For simplicity, we only express the pixel index (i,j) in the left part of the equation. Here, k(s) represents a normalized term, *p* denotes pixels within an *n*-by-*n* region Ω centered by s, $G_{\sigma_s}(p-s)$ describes the Gaussian kernel on spatial distance between the pixels *s* and *p*, $G_{\sigma_r}(C_p - C_s)$ indicates the Gaussian kernel on the intensity differences between the pixel *s* and *p*, and finally C_p represents the intensity at the pixel *p*. Both Gaussian kernel functions are with widths controlled by the standard deviation parameters σ_s and σ_r. In our implementation, we set the empirical value σ_s to cover a pixel neighborhood of between 24 and 48 pixels and σ_r is between 5 to 10% of the total pixel values in an HDR image, as suggested [13] [20]. For the Bush image, σ_s=3.0 and σ_r =4.25.

$$BF_s[C_n(i,j)] = \frac{1}{k(s)}\sum_{p\in\Omega} G_{\sigma_s}(p-s)\cdot G_{\sigma_r}(C_p - C_s)\cdot C_p.$$
$$k(s) = G_{\sigma_s}(p-s)\cdot G_{\sigma_r}(C_p - C_s). \quad (8)$$

Once the bilateral filter has derived the pixel value $BF_s[C_n(i,j)]$, we can develop the detail layer using Eq. (9), where $C_w(i,j)$ represents the luminance of the pixel (i,j) and a constant ε=10^{-6} is adopted to avoid the occurrence of singularity.

$$DL[C_w(i,j),\ C_n(i,j)] = \frac{C_w(i,j)+\varepsilon}{BF_s[C_n(i,j)]+\varepsilon}. \quad (9)$$

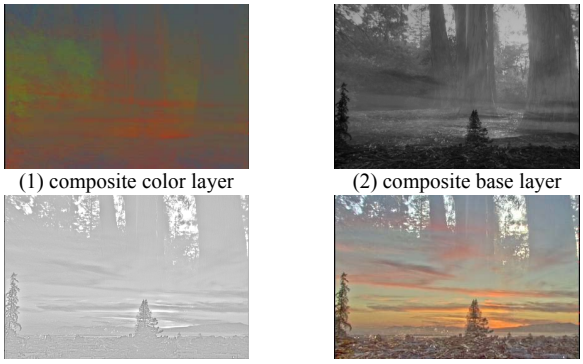

(1) composite color layer (2) composite base layer

(3) composite detail layer (4) the final composite image

Fig. 4. The composite results at each layer and the final composition image using the weight w_a=0.5 and w_b=0.5.

We show in Fig. 3 the detail layers for the Bush and Sunset images. We remark that the proposed algorithm combining the bilateral filter results with the original luminance provides a significant benefit in obtaining detailed information, even for the regions with similar luminance, such as the ground leaves in the Bush image and the edge of cloud in the Sunset image.

D. Image Feature Composition

We have described our approach to decompose an HDR image into three layers: color, base, and detail layers, where each layer preserves the corresponding information that has been normalized in a universal domain. The next step is to compose three features using the linear interpolation.

Without loss of generality, we assume that two HDR images, I_a and I_b, to be composed have the same image resolutions. In addition, we use suffices *a* and *b* to indicate the corresponding layer; namely, the color layer (CL), base layer (BL) and detail layer (DL). The composite results, denoted with the suffix *c* for each layer, can be expressed using Eq. (10), where w_a and w_b represent the weights employed for the HDR composition in each layer and $w_a + w_b = 1.0$.

$$\begin{aligned} \mathrm{CL_c}(i,j) &= \mathrm{w_a CL_a}(i,j) + \mathrm{w_b CL_b}(i,j). \\ \mathrm{BL_c}(i,j) &= \mathrm{w_a BL_a}(i,j) + \mathrm{w_b BL_b}(i,j). \\ \mathrm{DL_c}(i,j) &= \mathrm{w_a DL_a}(i,j) + \mathrm{w_b DL_b}(i,j). \end{aligned} \tag{10}$$

In the color layer, each pixel (i, j) is represented by the triple primary $[\mathrm{RCL_c}(i,j), \mathrm{GCL_c}(i,j), \mathrm{BCL_c}(i,j)]$. We can derive the influential ratios for the triple primary using Eqs. (11) and (12), which are similar to the expressions shown in Eqs. (1) and (2), where $\mathrm{CCL_c}(i,j)$ represents the colors appeared by the red, green, blue triple primary components.

$$\mathrm{CCL_c}(i,j) = \mathrm{RCL_c}(i,j) + \mathrm{GCL_c}(i,j) + \mathrm{BCL_c}(i,j). \tag{11}$$

$$\begin{aligned} \mathrm{r_c}(i,j) &= \mathrm{RCL_c}(i,j)/\mathrm{CCL_c}(i,j). \\ \mathrm{g_c}(i,j) &= \mathrm{GCL_c}(i,j)/\mathrm{CCL_c}(i,j). \\ \mathrm{b_c}(i,j) &= \mathrm{BCL_c}(i,j)/\mathrm{CCL_c}(i,j). \end{aligned} \tag{12}$$

The composite results for three layers are shown in Fig. 4(1) to 4(3). We can observe that each layer preserves crucial information corresponding to the composite HDR image.

E. HDR Map Estimation and Re-rendering

We have shown that we can employ the normalized information of each HDR image $\mathrm{C_n}(i,j)$ to form the composite base layer $\mathrm{BL_c}$. Unfortunately, the value domain of $\mathrm{BL_c}(i,j)$ does not belong to the HDR domain. As a result, we cannot re-render the composite result to produce n HDR image directly using the base layer. However, we can convert the $\mathrm{BL_c}(i,j)$ back to the HDR domain, $\mathrm{BL_{c\text{-}HME}}$, where the suffix HME means HDR map estimation. The conversion is accomplished using three steps.

First, we rewrite Eq. (7) and substitute the expression of $\mathrm{C_m}(i,j)$ using Eq. (5). The new equation is shown in (13), which is a quadratic equation with the variable $\mathrm{C_w}$ which represents the base layer to be determined.

$$\frac{\alpha^2}{\mathrm{C_{white}^2 C_{av}^2}}\mathrm{C_w^2} + \frac{\alpha}{\mathrm{C_{av}}}(1-\mathrm{C_n})\mathrm{C_w} - \mathrm{C_n} = 0 \tag{13}$$

The problem remained is that when four key constants, $\mathrm{C_{av}}$, $\mathrm{C_n}$, α, $\mathrm{C_{white}}$, are available, we are capable of solving $\mathrm{C_w}$ using the quadratic formula, as shown in Eq. (14).

$$\mathrm{C_w} = \frac{-\frac{\alpha}{\mathrm{C_{av}}}(1-\mathrm{C_n}) \pm \sqrt{\frac{\alpha^2}{\mathrm{C_{av}^2}}(1-\mathrm{C_n})^2 + 4\cdot\frac{\alpha^2}{\mathrm{C_{white}^2 C_{av}^2}}}}{\frac{2\cdot\alpha^2}{\mathrm{C_{white}^2 C_{av}^2}}} \tag{14}$$

Here, we describe in details how to determine four key constants. First, according to Banterle *et al.*'s experiments [2], the logarithmic average luminance in the original HDR image is similar to that shown in the tone-mapped LDR image. This means that we can estimate $\mathrm{C_{av}}$ using Eq. (4) by replacing the term $\mathrm{C_w}(i,j)$ by the current composite base layer, $\mathrm{BL_c}(i,j)$.

Second, the concept of the tone mapping techniques is to map the smallest and largest luminance values into the range [0, 1]. Therefore, when $\mathrm{C_w}$ is approaching to the infinity ($\mathrm{C_w} \to \infty$), the output value of tone-mapped value equals the upper bound of the displayable value, which is normally set to be 1. Thus, we let $\mathrm{C_n}$ = 1 in our implementation and simplify Eq. (14) to become Eq. (15). Note that since the color values are positive, we only employ the positive part in the quadratic formula. We set $\mathrm{C_{w\to\infty}}$ to be the maximal value in the base layer; i.e., $\mathrm{C_{w\to\infty}} = \max[\mathrm{BL_c}(i,j)]$ for all pixels (i, j), where the function max[] reports the maximum for all pixels (i, j) in the base layer of the composite HDR image.

$$\mathrm{C_{w\to\infty}} = \frac{\mathrm{C_{white}C_{av}}}{\alpha} \tag{15}$$

Third, Banterle *et al.* suggested that $\mathrm{C_{white}}$ can be any value between the smallest and middle values of the luminance value [2] [12] [15]. We adopt $\mathrm{C_{white}}$ as the mean value between the smallest and the middle values balancing the smallest and middle values without incurring any bias to both values. Finally, we are able to estimate the α value using Eq. (16) since $\mathrm{C_{w\to\infty}}$, $\mathrm{C_{white}}$, and $\mathrm{C_{av}}$, have been estimated properly.

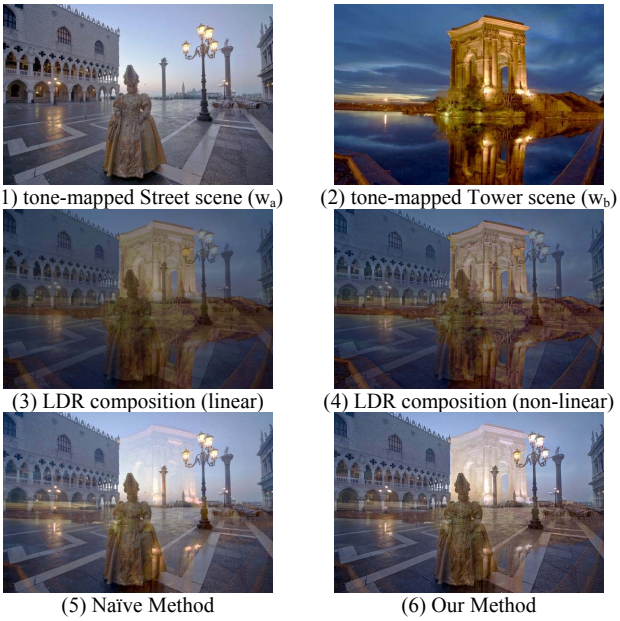

Fig. 5. Tone-mapped images Street (1) and Tower (2). The linear LDR composition using w_a=0.3 and w_b=0.7 (3) and that using the non-linear interpolation suggested in [6] is shown in (4). The naïve HDR compossition (5). The composition using our proposed algorithm 6). Our scheme preserves contrast and colors producing the best visually plausible and informative images outperforming other approaches.

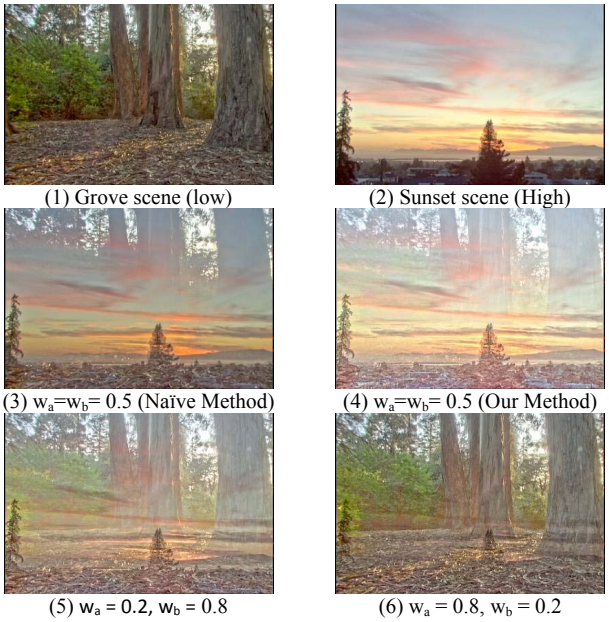

Fig. 6. The comparison of HDR composition results. The naïve HDR composition is influenced by the high exposure image (3). Our algorithm balances the low and high exposures (4), thus producing a more informative composition result corresponding to different weights (5) and (6).

$$\alpha = \frac{C_{white} C_{av}}{\max[BLc(i,j)]} \tag{16}$$

We have shown so far that we have determined constants needed allowing us to solve C_w using Eq. (17), which accomplishes the task of the HDR map estimation by assigning the value of BL_{c-HME}.

$$C_w = BL_{c-HME} \tag{17}$$

The final process we need to conduct is to re-render the HDR composite image. Referring to the influential ratios, $r_c(i,j), g_c(i,j), b_c(i,j)$ shown in Eq. (12), we can compute the new value in the red, green, and blue channel using Eq. (18), where $DL_c(i,j)$ represents the corresponding value in the detail layer. This accomplishes the re-rendered process and generates the final composite HDR image, where each pixel (i,j) has the new values $[R'_w(i,j), G'_w(i,j), B'_w(i,j)]$.

$$\begin{aligned} R'_w(i,j) &= r_c(i,j) \times C_w \times DL_c(i,j) \\ G'_w(i,j) &= g_c(i,j) \times C_w \times DL_c(i,j) \\ B'_w(i,j) &= b_c(i,j) \times C_w \times DL_c(i,j) \end{aligned} \tag{18}$$

The re-rendered composite HDR image is shown in Fig. 4(4). We employ an equal weight in this example, and thus the information appearing in the final result approximately reveals half of the saliency from both images. This example also demonstrates that our algorithm is capable of producing a final HDR image composed by the low exposure and high exposure using the linear interpolation.

IV. Experimental Results

We implemented our algorithm using the C++ programing language and collect our experiments on a personal computer platform. We have shown in Fig. 3 the HDR composition image using the low exposure and high exposure. We demonstrate in Fig. 5 an example of using Street and Tower HDR images with the low exposure for composition.

First, the tone-mapped images using the Luminance HDR software are shown in Figs. 5(1) and (2). Fig. 5(3) shows the LDR composition result which applies the linear interpolation method to two tone-mapped LDR images using the weight w_a=0.3 and w_b=0.7. Fig. 5(4) shows the LDR composition result which applies the non-linear method [6]. In contrast, we show in Fig. 5(5) the HDR composition result which applies the linear interpolation directly on two HDR images, which is referred to as a naïve method. Since the result is an HDR image, we need to operate the tone mapping for visualization. Note the composition result shows little details from the Tower image, even we exert the influence using a large weight (w_b=0.7). Finally, Fig. 5(5) shows the HDR composition result generated by our proposed algorithm using three processes described in previous section. Comparing to the appearance of the composition results shown in Fig. 5(5), our method preserves more saliency in contrast and colors.

Figs. 5(3) and 5(4) do not present a proper composition results because they adopt the tone-mapped LDR image for composition which inevitably loses contrast and details. In contrast, Fig. 5(5) shows a more interesting result by adopting the HDR images and the naïve method for composition. However, since we use the weight w_b=0.7, we expect more detailed information of the Tower image should appear in the resultant composition HDR image. Fig. 5(6) presents the best performance of the HDR composition, where contrast and details are preserved. These results demonstrate the superiority of our proposed algorithm in preserving contrast, colors, and details during the composition process.

(1) (2) (3)

(4) An HDR composition image using (1) and (2)

(5) An HDR compostion image using (1) and (3)

Fig. 7. Two HDR composition images produced by our algorithm using weights w_a=0.6 and w_b=0.4.

Fig. 6 shows another comparison result. Two HDR images to be processed are with the low exposure and high exposure. Despite of using the same weights, w_a=w_b=0.5, the composition image produced by the naïve method is influenced by the high exposure image. In contrast, when using our proposed HDR composition algorithm, the generated composition shows a balance between the low and high exposure producing a more informative composition results. Figs. 6(5) and 6(6) show our composition images using different weights which emphasize different contributions by both images.

Fig. 7 demonstrates two HDR composition images using our algorithm. These two images demonstrate that our algorithm faithfully produces the composition results using the linear interpolation corresponding to the given weights. The composition images being produced look like a tone-mapped image from a real scene producing a meaningful image for artistic and esthetic rendition.

V. Conclusions and Future Work

We present a novel algorithm for HDR image composition using the linear interpolation. Our scheme first decomposes HDR images into three layers: color layer, base layer, and detail layer. Then, we produce the composite result at each layer independently using a linear interpolation with desired weights. Finally, we estimate an HDR map and re-render the composite result by referring to the base layer to produce the final HDR composition image. Experimental results show that our algorithm preserves the saliency of the contrast and colors producing visually plausible HDR composition image. The comparison shows that our algorithm provides better results than those generated by the current state-of-the-art LDR image composition and the naïve HDR composition method. We consider our scheme extend HDR applications producing a meaningful image for artistic and esthetic rendition.

Future work includes extending our algorithm to investigate HDR image stitching, HDR image fusion, HDR videos, or HDR watermarking [10] [11].

Acknowledgment

This work was supported by the Ministry of Science and Technology, Taiwan, under Grant MOST 104-2221-E-005-026-MY3. C. M. Wang's research was supported in part by Taiwan Information Security Center (TWISC), Academia Sinica, and Ministry of Science and Technology, Taiwan, under the grant MOST 104-2218-E-001-002.

References

[1] A. Adams, *The Negative* (Ansel Adams Photography, book 2), Ansel Adams Publisher, June 1995.

[2] F. Banterle, P. Ledda, K. Debattista, and A. Chalmers, "Inverse tone mapping," in *Proceedings of the Fourth International Conference on Computer Graphics and Interactive Techniques in Australasia and Southeast Asia*, pp. 349-356, ACM Press, December 2006.

[3] F. Durand and J. Dorsey, "Fast bilateral filtering for the display of high-dynamic-range images," *ACM Transactions on Graphics*, vol. 21, iss. 3, pp. 257-266, 2002.

[4] G. Eilertsen, R. K. Mantiuk, and J. Unger, "Real-time noise-ware tone mapping," *ACM Transactions on Graphics*, vol. 34, iss. 6, article no. 198, Nov. 2015.

[5] R. C. Gonzalez and R. E. Woods, *Digital Image Processing*, Third Edition, Prentice Hall, 2007.

[6] M. Grundland, R. Vohra, G. P. Williams, and N. A. Dodgson, "Cross dissolve without cross fade: preserving contrast, color and salience in image compositing," *Computer Graphics Forum*, Vol. 25, No. 3, pp. 577-586, 2006.

[7] M. Grundland, R. Vohra, G. P. Williams, and N. A. Dodgson, "Non-linear multiresolution image blending," *Machine Graphics and Vision International Journal*, vol. 15, iss. 3, pp. 381-390, Feb. 2006.

[8] P. Hanhart, M. V. Bernardo, M. Pereira, A. M. G. Pinheiro, and T. Ebrahimi, "Benchmarking of objective quality metrics for HDR image quality assessment," *EURASIP Journal on Image and Video Processing*, vol. 39, pp. 1-18, 2015.

[9] C. Lee, Y. Li, and V. Monga, "Ghost-free high dynamic range imaging via rank minimization," *IEEE Signal Processing Letters*, vol. 21, no. 9, pp. 1045-1049, September 2014.

[10] E. Maiorana and P. Campisi, "Multi-bit watermarking of high dynamic range images based on perceptual models," *Security and Communications Networks*, doi: 10.1002/sec. 1345, 2015.

[11] E. Maiorana and P. Campisi, "High-capacity watermarking of high dynamic range images," *EURASIP Journal on Image and Video Process.* 2016:3, doi:10.1186/s13640-015 -0100-7, 2016.

[12] L. Meylan and S. Süsstrunk, "High dynamic range image rendering using a retinex-based adaptive filter," *IEEE Transactions on Image Processing*, Vol. 15, No. 9, pp. 2820-2830, 2006.

[13] G. Petschnigg, R. Szeliski, M. Agrawala, M. Cohen, H. Hoppe, and K. Toyama, "Digital photography with flash and no-flash image pairs," *ACM Transactions on Graphics*, vol. 23, iss. 3, pp. 664-672, 2004.

[14] E. Reinhard G. Ward, S. Pattanaik, P. Debevec, W. Heidrich, and K. Myazkowski, *High Dynamic Range Imaging: Acquisition, Display, and Image-based Lighting*, second edition, Morgan Kaufmann, 2010, pp. 103-104.

[15] A. G. Rempel, M. Trentacoste, H. Seetzen, D. Young, W. Heidrich, L. Whitehead, and G. Ward, "Ldr2hdr: on-the-fly reverse, tone mapping of legacy video and photographs," *ACM Transactions on Graphics*, ol. 26, No. 3, Article 39, 2007.

[16] R. Szeliski, "Image alignment and stitching: a tutorial," *Foundations and Trends in Computer Graphics and Vision*, vol. 2, iss. 1, pp. 1-104, January 2006.

[17] Z. Wang, D. Ziou, C. Armenakis, D. Li, and Q. Li, "A comparative analysis of image fusion methods," *IEEE Transactions on Geoscience and Remote Sensing*, vol. 43, iss. 6, pp. 1391-1402, June 2005.

[18] T. H. Wang, C. W. Chiu, W. C. Wu, J. W. Wang, C. Y. Lin, C. T. Chiu, and J. J. Liou, "Pseudo-multiple-exposure-based tone fusion with local region adjustment," *IEEE Trans. Multimedia*, vol. 17, no. 4, pp. 470-484, April 2015.

[19] C. M. Yu, K. C. Wu, and C. M. Wang, "A distortion-free data hiding scheme for high dynamic range images," *Displays*, vol. 32, pp. 225-236, 2011.

[20] C. Zhou, A. Troccoli, and K. Pulli, "Robust stereo with flash and no-flash image pairs," in *Proceedings of 2012 IEEE Conference on Computer Vision an Pattern Recognition (CVPR)*, pp. 342-349, 2012.